

MODELING OF THE HUMAN EXPOSURE INSIDE A RANDOM PLANE WAVE FIELD

F. Moglie, V. Mariani Primiani, and A. P. Pastore

Dipartimento di Ingegneria Biomedica, Elettronica
e Telecomunicazioni
Università Politecnica delle Marche
Via Brecce Bianche 12, Ancona 60131, Italy

Abstract—The specific absorption rate (SAR) of a human body exposed to a random field inside a reverberation chamber (RC) has been modeled. The exciting field is simulated using the plane wave integral representation which is numerically solved by a superposition of N plane waves randomly generated and repeated M times to reproduce the same statistics of an RC. An experimental validation, carried out by means of known saline solutions, confirms the reliability of this method. The obtained results at various frequencies for the adopted “Visible Human Body” and for some tissues well highlight the absorption percentage. The frequency behavior of the total SAR reveals the resonance of the human body around 75 MHz, in spite of the chaotic source.

1. INTRODUCTION

The analysis of the interaction between electromagnetic fields and the human body is of particular interest for the scientific community. The growing use of personal communication devices has recently led several studies on this topic. Therefore, the SAR distribution in the head of a human exposed to the electromagnetic field emitted from hand-held portable radios and hand-held cellular phones were investigated. In [1] also the temperature increment inside the head of a cellular phone user was evaluated. The SAR computation in human head has also been done applying analytical methods based on the complex image theory [2]. A lot of investigations have been made on simple tissues, that are commonly available for experimental results analyzing the

dielectric properties of tissues and their equivalent liquids. Dielectric properties are of fundamental importance for the calculation of power deposition in human tissues [3]. Of course, studies using virtual models of the whole human body were also carried out. For example in [4] a finite difference time domain (FDTD) method for analysis of an anatomically based heterogeneous man model exposed to ultra wide-band electromagnetic pulse sources was proposed.

Numerical modeling has been also used to check practical solutions for the reduction of peak SAR in human head due to handset phones [5]. Whole body analysis is a key point especially to correctly relate exposure reference level and basic restrictions [6], especially when core temperature elevation must be estimated from whole-body averaged specific absorption rate (WBA-SAR) [7]. All these numerical dosimetry analyses were made using a single plane wave that impinges on the analyzed biological body [8]. More recently, the necessity to reproduce a realistic environment, where potentially dangerous radiation may come from any direction, led to the use of an RC to randomize the exposure.

The idea of using RCs for animal exposure to electromagnetic fields was first suggested by the National Institute of Standards and Technology (NIST) in a special session at Bioelectromagnetics Society (BEMS) annual meeting in 2001. A preliminary study, involving an experimental investigation, was performed by NIST, and a preliminary numerical dosimetry study was performed by the Foundation for Research on Information Technologies in Society (IT'IS), both funded by the National Institute of Environmental Health Sciences (NIEHS) in the USA. The results of this preliminary study were very encouraging, and in January 2006, the main study to evaluate the potential toxicity and carcinogenicity of cell phone RF radiation in laboratory animals was issued by NIEHS under the national toxicology program (NTP). These results constitute the outcome of the chamber prototype development and evaluation phase of the study [9].

Beside the use of RC for testing mobile phone antennas [10], this electromagnetic facility has been used to expose animals at WiFi [11] and global system for mobile communications (GSM) [12] frequencies. In vitro experiments and FDTD simulations were also carried out on biological materials in an RC at 900 MHz [13]. Recently the RC was proposed to assess the whole human body exposure to mobile phone frequencies [14]. The present paper describes numerical computation of the SAR of a whole human body exposed to a random field. The source is not considered in contact with the body, but placed at far field. In this way we simulated the presence of a person inside a resonant environment excited by a generic source. Three situations

may occur: 1) the source is moving inside the environment and the person is at fixed position; 2) the source is fixed and the person moves inside the chamber; 3) both source and person are moving. In each case, the person is exposed to a variable field, determining a stochastically variable exposure [15, 16]. The possibility to simulate all these situations represents the significance and practical importance of the problem that is considered in the paper. On the other hand, the static configuration where the source, the person, and the environment are fixed is less frequent in realistic cases.

This kind of electromagnetic field is well representable by means of an RC. The human body is represented by the “Visible Human Body Project” model [17]. It is placed in an RC whose internal field is simulated using the plane wave integral representation (of an RC) [18], and numerically solved by a superposition of N plane waves repeated M times to simulate M independent stirrer positions. For each plane wave set, the body absorbed power is computed, and then the averaged SAR is achieved.

2. DESCRIPTION OF THE METHOD

Inside a well operating RC, the field is statistically uniform, isotropic and depolarized. Considering an object placed inside the RC, whose operation is accomplished by a mechanical stirrer, the complex field distribution created inside the chamber by each stirrer position is modeled by a superposition of random plane waves.

The method is described in [19], and it is based on the use of the plane wave integral representation for an RC that is approximated by a finite summation of plane wave contributions. Therefore, the chamber was substituted by a superposition of plane waves, each one with statistically variable polarization and phase. It is possible to change the field distribution, as happens inside a real chamber when the stirrer position is changed, by simply changing the values of the parameters of each plane wave. The only parameters that describe characteristics of the chamber are N and M . N represents the number of plane waves excited in order to simulate the field distribution in the chamber for a particular position of the stirrer. Then, the simulation is repeated M times, where M is the number of independent positions of the stirrer in the chamber. In fact, another important aspect that has to be modeled to reproduce the RC field is the ability of the stirrer to change the field boundary conditions during its rotation, and therefore the field distribution inside the chamber, that is quantified in terms of its statistically independent positions [20]. The higher M is the better are the field properties in terms of uniformity and

isotropy. From a practical point of view, a minimum value for M is required, as function of the frequency and the chamber's dimensions, to guarantee acceptable field properties [21]. We choose these parameters as a compromise between the computation time and the statistical convergence of the central limit theorem and of the law of large numbers. With FDTD it is not necessary to simulate the entire volume of the chamber, but only a volume which is a bit more than the volume of the analyzed object. This is done by a proper placement of absorbing boundary conditions (ABCs) and the separation planes between the total field zone and the scattered field zone. Perfectly matched layer (PML) ABCs [22] were used to terminate the computational volume. Furthermore, in order to recreate the exact behavior of the chamber it is necessary to verify a relationship between the total average field in the chamber $\langle |\vec{E}_T| \rangle$ and the amplitude of each plane wave E_0 [23]

$$\langle |\vec{E}_T| \rangle = \frac{15}{16} E_0 \sqrt{\frac{\pi}{3}} \sqrt{N} \quad (1)$$

This relationship between the averaged total field and the amplitude E_0 of each plane wave is very useful to correlate simulations and measurements. After a measurement in an RC of the averaged (over the stirrer rotation) total field amplitude $\langle |\vec{E}_T| \rangle$, it is possible to simulate the field inside the chamber by M sets of N plane waves, assigning them the constant amplitude E_0 according to Equation (1).

In order to simulate the realistic behavior of the chamber, it is necessary to generate M sets of plane wave summation, but statistically independent of each other. This can be accomplished by a proper choice of the parameters of each plane wave, considering the field properties inside an ideal chamber.

The parameters of each plane wave are generated at the FDTD initialization step. They are stored and recalled for at each FDTD temporal iteration. Referring to Figure 1 the generated parameters are: the angles θ and φ , the distance d , and polarization α . The polarization α is the angle between the electric field vector and the vertical plane defined by the z -axis and the angle φ . More precisely, φ , d , and α exhibit a uniform distribution, whereas a sinusoidal distribution was chosen for θ . This choice ensures that the propagation directions are uniformly distributed over the solid angles.

Inside an ideal chamber the field does not exhibit a preferred propagation direction, being the signal, launched by a transmitting antenna, reflected (theoretically for infinite times) by the walls and the stirrer (ideal conductors). This means that the propagation angles have the same probability over the solid angles (uniform distribution). To explain that, a spherical surface surrounding the field observation

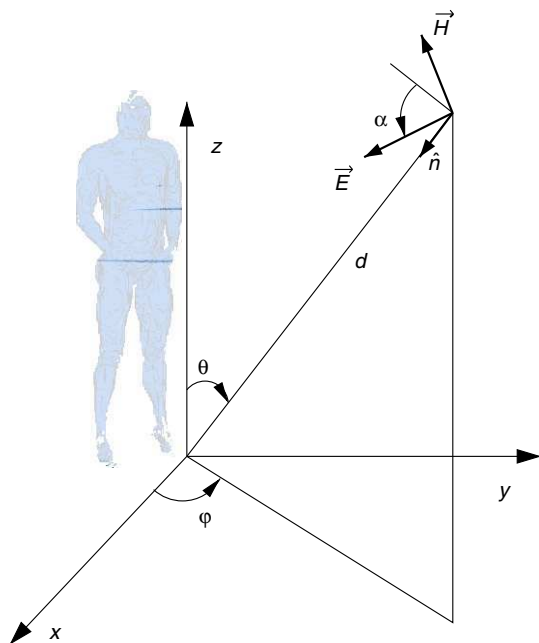


Figure 1. Geometry of a random plane wave incident on the computation volume.

point located at the center of the reference system can be introduced. For each plane waves set, N points of the sphere can be associated to N impinging directions of the plane waves, and in order to represent the RC field, they must be uniformly distributed on the surface itself. A uniform distribution for both angles θ and ϕ would result into a strong gathering of the propagation directions when θ approaches 0° and 180° . For example, considering the extreme values $\theta = 0^\circ$ and $\theta = 180^\circ$, we achieve the same incident direction for any ϕ , whereas for $\theta = 90^\circ$ we have many impinging directions. To reach the goal, a uniform distribution can be chosen for ϕ so that its probability density function (PDF) becomes

$$\text{PDF}(\phi) = \begin{cases} 1/(2\pi) & \text{for } 0 \leq \phi \leq 2\pi \\ 0 & \text{else} \end{cases} \quad (2)$$

whereas for θ the probability density decreases towards the poles

$$\text{PDF}(\theta) = \begin{cases} 0.5 \sin(\theta) & \text{for } 0 \leq \theta \leq \pi \\ 0 & \text{else} \end{cases} \quad (3)$$

Equations (2) and (3) ensure that the propagation directions are uniformly distributed over the solid angles. The second important field

property in an RC is the absence of a preferred polarization due to the multiple scattering operated by the stirrer during its rotation. This leads to the assumption of a uniform distribution for the polarization angle α in the range $[0, 2\pi]$. As regards the phase γ of the single wave, the choice of a uniform distribution between 0 and 2π seems to be the most suitable to replicate a real chamber condition due to the wall multiple reflections.

A particular care is required in the generation of θ starting from a uniform distribution. According to the theory of statistical functions [24], we can achieve a PDF from the uniform distribution if the corresponding cumulative distribution function (CDF) can be inverted. Denoting with u a uniform distribution in $[0, 1]$, from (3),

$$\text{CDF}(\theta) = \begin{cases} \int_0^\theta \frac{\sin(x)}{2} dx = u & \text{for } 0 \leq \theta \leq \pi \\ 0 & \text{else} \end{cases} \quad (4)$$

so that for $0 \leq \theta \leq \pi$

$$\int_0^\theta \frac{\sin(x)}{2} dx = 0.5(1 - \cos(\theta)) = u \quad (5)$$

$$\theta = \arccos(1 - 2u) \quad (6)$$

In all other cases the distribution is uniform and

$$a = 2\pi u \quad (7)$$

where the angle a denotes the azimuth φ , or the polarization α , or the plane wave phase γ . The function u was generated by the `rand()` function of C language.

The statistical independence of the generated waves is numerically ensured by the pseudo-random number generator function of the C language. Statistically, it is possible that inside an RC two plane waves have two very close directions, but from a physical point of view they are generated by a great number of different combined reflections from the walls and the stirrer (designed to this purpose with high reflecting material). In other words, before impinging the body, the two waves have traveled inside the RC along completely different paths and this aspect gives to the two waves a statistical independence of the phase and of the polarization. Beside the above described situation, where the excitation is completely random and characterized by a Rayleigh distribution, it is also possible to account for the presence of a certain direct illumination of the body produced by the transmitting antenna. In this case, the field statistical distribution moves toward a Rice type, and the simulation can be accomplished by adding some direct plane waves to include a line of side (LOS) illumination [25].

3. SIMULATED VISIBLE HUMAN BODY

The human model was built from images of the well known “Visible Human Body Project” available from the Internet [17]. 29 images were used to obtain a discrete model with a resolution of 10 mm. The dimensions of the model are $0.57 \times 0.29 \times 1.87 \text{ m}^3$ and there are 33 different tissues. Then the relative permittivity ϵ_r and the conductivity σ were assigned to every tissue. They can be automatically recovered by a computation program with an algorithm that implements the Cole-Cole law for desired frequencies and tissues. Parameters contained in the equation are described and recovered by [26] fitting measurements directly made on 44 biological tissues from 10 Hz up to 20 GHz. Most parameters in the Cole-Cole equation are estimated from animal tissues and often postmortem, so it is possible to have the approximate conductivity profile for every frequency of the entire human body, including all organs and tissues. For example in Figure 2 the conductivity profile at a frequency of 75 MHz is shown. The same Figure 2 shows the reference coordinate system. The whole FDTD grid has the human body model in the center. A total field layer of 25 cells surrounds the human body model. Then there are separation planes where the plane waves are excited. A reflected field layer of 25 cells surrounds the separation planes. At the end, PML

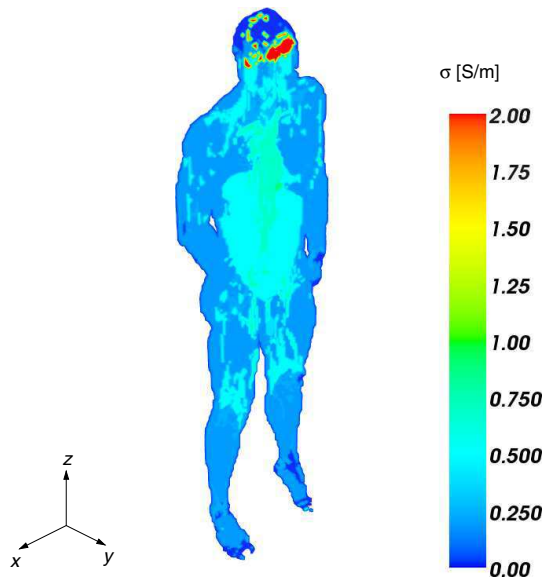


Figure 2. Conductivity profile at the frequency of 75 MHz.

ABCs of 8 cells and parabolic conductivity terminate the grid.

The field inside the body is computed for each i -th plane wave excitation, and then the local SAR produced by the j -th plane wave set is obtained by the electric field values \vec{E}_i

$$\text{SAR}_j = \frac{\sigma}{2\rho} \left| \sum_{i=1}^N \vec{E}_i \right|^2 \quad (8)$$

where σ (S/m) is the conductivity and ρ (kg/m³) the density of the tissue. The ensemble averaged, over the M plane wave sets (equivalent to the ensemble average over the stirrer rotation), SAR is simply given by

$$\langle \text{SAR} \rangle_M = \frac{1}{M} \sum_{j=1}^M \text{SAR}_j \quad (9)$$

The SAR was calculated in a precise way for the entire body, taking into account the σ dependency on the frequency.

After a proper analysis [19], we chose $N = 100$ and $M = 200$. We used the fixed frequencies of 25 MHz, 50 MHz, 62.5 MHz, 75 MHz, 87.5 MHz, 100 MHz, 125 MHz, 150 MHz, 175 MHz, 200 MHz and the simulations were performed for 20 periods. The cell size was 10 mm. The computation volume was the human body volume with 30 cells added at the beginning and at the end of each axis for the separation planes and absorbing boundary conditions.

With the adopted discretization, the FDTD modeling of the human body is strictly valid up to the frequency of 100 MHz. The tissue which has the shortest wavelength is the liquor and at this frequency the wavelength is about 0.2 m. It is commonly accepted that the cell side of the $\lambda/20$ gives accurate results, but accepting a little less accuracy we can extend the frequency range up to 200 MHz. In the last period, when a steady state was reached, we evaluated the magnitude of the electric field for each cell.

4. EXPERIMENTAL VALIDATION OF THE MODEL

In order to experimentally validate the model, a measurement of the S_{21} parameter between the transmitting antenna and a monopole immersed in a NaCl solution has been carried out.

A plastic box of $210 \times 150 \times 100$ mm³ was fabricated and filled with the saline solution with three different normalities: 0.0N, 0.085N, and 0.267N. The normality of a solution is the number of gram equivalent weight of a solute per liter of its solution. Their dielectric parameters have been calculated on the basis of an interpolating formula [27].

Table 1. Dielectric properties of the NaCl solutions at different frequencies [27].

Solution	800 MHz	900 MHz	1000 MHz
$N = 0.0$	$\epsilon_r = 78.2;$ $\sigma = 0.13 \text{ S/m}$	$\epsilon_r = 78.2;$ $\sigma = 0.17 \text{ S/m}$	$\epsilon_r = 78.2;$ $\sigma = 0.21 \text{ S/m}$
$N = 0.085$	$\epsilon_r = 76.6;$ $\sigma = 0.99 \text{ S/m}$	$\epsilon_r = 76.5;$ $\sigma = 1.03 \text{ S/m}$	$\epsilon_r = 76.5;$ $\sigma = 1.07 \text{ S/m}$
$N = 0.267$	$\epsilon_r = 73.2;$ $\sigma = 2.74 \text{ S/m}$	$\epsilon_r = 73.1;$ $\sigma = 2.77 \text{ S/m}$	$\epsilon_r = 73.1;$ $\sigma = 2.81 \text{ S/m}$

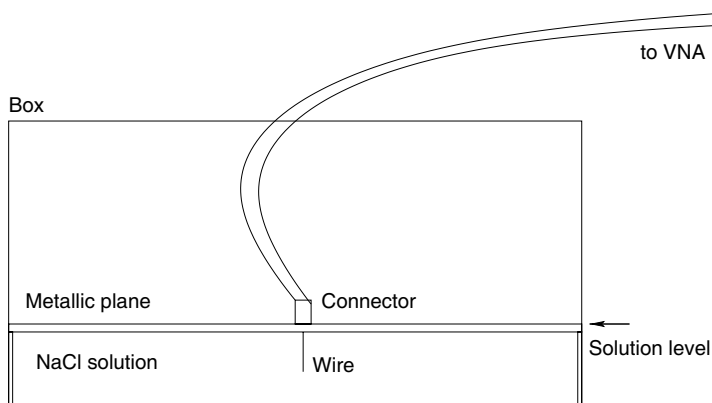


Figure 3. Plastic box placed in the working volume of the RC. It is filled with the NaCl solution up to a height of 30 mm. A metallic plane with the 18 mm monopole was immersed in the solution and connected to VNA port 2.

Table 1 reports the permittivity and conductivity values corresponding to the saline solutions: $N = 0.0$ means distilled water.

The box described in Figure 3 was placed in the working volume of an RC. The monopole was implemented using the central conductor of a type N connector for panel mounting. The total length of the monopole is 18 mm, while the dimensions of the ground plane are $210 \times 150 \text{ mm}^2$. Figure 4 shows the RC setup: dimensions are $6.00 \times 4.00 \times 2.50 \text{ m}^3$. Two stirrers were placed along the y (paddle shape) and z (Z-folded shape) axes, and the plastic box filled with the saline solution was placed above a 1 m height polystyrene support inside the working volume.

The transmitting antenna is a log-periodic, from 300 MHz to 5 GHz (Schwarzbeck model USLP 9143). A vector network analyzer

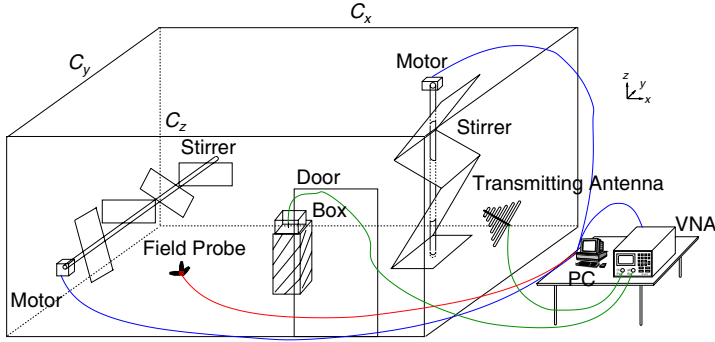


Figure 4. Chamber, stirrers and box. The dimensions of the chamber are $C_x = 6.00$ m, $C_y = 4.00$ m, and $C_z = 2.50$ m.

(VNA) (Agilent Technologies E5071B) is used to measure the voltage on the monopole immersed in the saline solution by the measurement of the transmission coefficient. The chamber works in a stirred mode. The rotation time is 80 s and the sampling rate is determined by the 1601 VNA sweep points. The VNA works in continuous wave mode, and the sweep time is equal to the stirrer rotation time. Measurements were repeated changing the frequency with a step of 250 kHz. The total average electric field, used in the simulations, has been measured by a tri-axial field sensor (Holaday HI 6005). The saline solution height in the box was 30 mm. The monopole was connected to VNA port 2 and the transmitting antenna was connected to the VNA port 1. We reproduced the same setup in a simulation with a box of $195 \times 162 \times 94$ cells with a cell size of 2 mm. The transition between the coaxial line and the monopole was accurately modeled according to [28].

In Figure 5 the comparison between experimental and simulated results is shown. The working frequency is around 900 MHz where our RC works well. The length of the dipole and box dimensions were chosen to give us a better sensitivity at this frequency. We can note that numerical results match measurements also considering the combined uncertainties in the measurements. The derivation of total uncertainty requires to include both experimental and numerical components. In experiments, the chamber electric field and the monopole output voltage are required. The field sensor exhibits a ± 1.5 dB (rectangular distribution) uncertainty. Regarding the output voltage, it is measured starting from the S_{21} value and from the

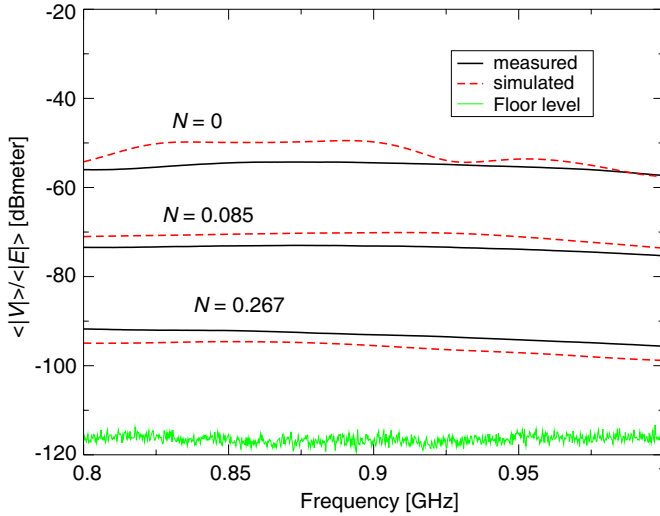


Figure 5. Simulated and measured results for the different NaCl solutions.

knowledge of the VNA output power measured by a spectrum analyzer:

$$V_{out} = S_{21} \sqrt{50P_{inc}} \tag{10}$$

We neglect the residual error in VNA measurements after the calibration procedure, whereas the uncertainty given by the spectrum analyzer power measurement was ± 1.5 dB (rectangular distribution). Moreover, the reverberation chamber field exhibits a non uniformity inside the working volume. The IEC standard [21] requires a standard deviation of no more than ± 3 dB in the considered frequency range. Our chamber is able to ensure a value of ± 1.5 dB. As far as simulations concerns, the chosen N and M values ensure a ± 1 dB of standard deviation, as shown in [19] where we analyzed uniformity and convergence of the applied method. Combining all terms, according to standard procedures [29], and applying a coverage factor of 2 to achieve a 95% of confidence level, we get a total combined uncertainty of ± 4.36 dB. The previous analysis does not consider uncertainty in saline solution preparation.

5. RESULTS

The simulations were run on an IBM BCX/5120 computer cluster, using 200 CPUs in 18 hours in the case of $f = 75$ MHz. The whole FDTD volume is $173 \times 145 \times 303$ cells. It includes the human body

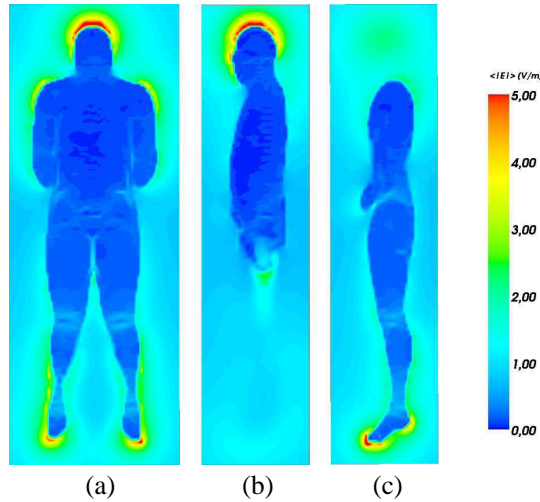


Figure 6. Electric field at the frequency of 75 MHz. (a) x - z plane at $y = 0.19$ m, (b) y - z plane at $x = 0.38$ m, and (c) y - z plane at $x = 0.24$ m.

model, the total and reflected field zones, and the PML ABCs. The developed code is able to return the field distribution inside the body in all sections. For example, Figure 6 reports the field map at 75 MHz for different sections. Electric field values are obtained setting $|\vec{E}_T| = 1$ V/m in the simulations, so that the amplitude of each plane wave is $E_0 = 0.104$ V/m according to Equation (1). Due to the linearity of the model, results can be scaled for any other field values required by human exposure standards. In Figure 7 the corresponding averaged SAR is shown in the same body sections. In Figure 8, the values of the total absorbed power in all tissues of the body are reported as function of frequency.

The highest total absorbed power value occurs around 75 MHz, which corresponds to the resonant frequency of the body if considered a receiving antenna. It is important to note that inside an RC, even if the exciting field has random properties, the response exhibits resonances strictly related to the frequency response of the device under test [28, 30]. This happens for the human body too, as obtained results demonstrate. This human whole body resonance is close to the frequency range used for frequency modulation (FM) broadcasting, but far from GSM and WiFi frequencies. In Table 2, the values for the ρ SAR in some individual tissues at the previously analyzed frequencies have been collected.

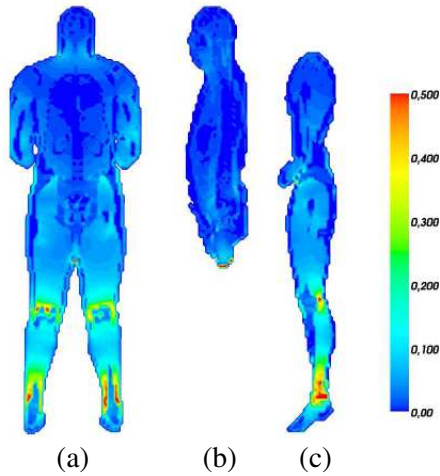


Figure 7. ρ SAR at the frequency of 75 MHz in $[W/m^3]$. (a) $x-z$ plane at $y = 0.19$ m, (b) $y-z$ plane at $x = 0.38$ m, and (c) $y-z$ plane at $x = 0.24$ m.

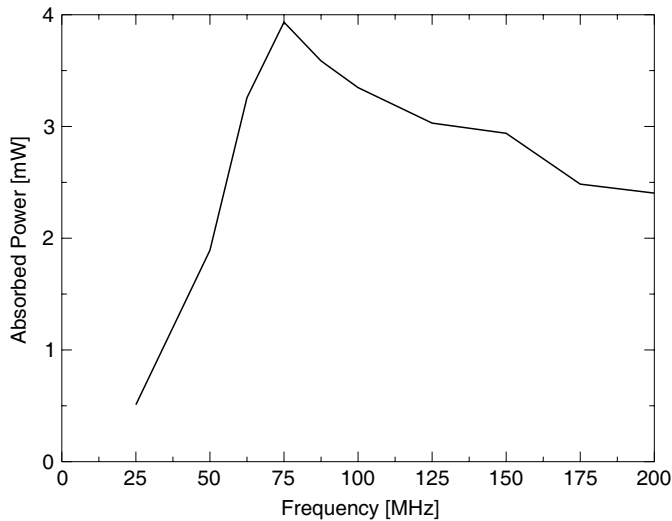


Figure 8. Total absorbed power for the whole body in the frequency domain.

Table 2. Percentage of ρ SAR for some tissues.

Name	25 MHz	50 MHz	62.5 MHz	75 MHz	87.5 MHz
Fat	2.36%	2.46%	2.45%	2.59%	2.83%
Lax Connective	4.79%	4.85%	4.86%	4.75%	4.58%
Compact Bone	2.63%	2.40%	2.38%	2.24%	2.21%
Dense Connective	3.38%	2.96%	2.89%	2.71%	2.62%
Subcutaneous Connective	20.64%	20.42%	20.37%	20.40%	21.26%
Intestine Cavities	2.60%	2.63%	2.48%	2.27%	2.05%
Muscle	59.32%	59.60%	60.06%	60.66%	60.50%
Name	100 MHz	125 MHz	150 MHz	175 MHz	200 MHz
Fat	3.05%	2.91%	2.85%	3.09%	3.28%
Lax Connective	4.43%	4.04%	3.79%	3.73%	3.57%
Compact Bone	2.09%	2.12%	2.10%	1.99%	1.91%
Dense Connective	2.43%	2.31%	2.12%	1.92%	1.76%
Subcutaneous Connective	21.63%	22.38%	23.06%	23.54%	24.38%
Intestine Cavities	1.86%	1.64%	1.50%	1.52%	1.52%
Muscle	60.38%	59.92%	59.08%	58.29%	57.32%

6. CONCLUSION

The RC field is very similar to the real world where potential dangerous radiations can come from different directions and polarizations. The electric field inside a human body model exposed to a random field was accurately determined. The random field produced by an RC has been modeled by a plane wave superposition.

An FDTD code was adopted to solve the sub-problem of the interaction between a plane wave and a non-homogeneous and lossy material. Subsequently, SAR values were computed for each tissue depending on the knowledge of permittivity parameters. The

numerical code was experimentally validated using saline solutions.

The achieved results highlight that, even if in presence of a chaotic excitation, the total SAR maintains the frequency response forced by the human body dimensions.

REFERENCES

1. Wang, J. and O. Fujiwara, "FDTD computation of temperature rise in the human head for portable telephones," *IEEE Trans. Microw. Theory Tech.*, Vol. 47, No. 8, 1528–1534, Aug. 1999.
2. Omar, A. A., "Complex image solution of SAR inside a human head illuminated by a finite-length dipole," *Progress In Electromagnetics Research B*, Vol. 24, 223–239, 2010.
3. Caputa, K., M. Okoniewski, and M. A. Stuchly, "An algorithm for computations of the power deposition in human tissue," *IEEE Antennas Propag. Mag.*, Vol. 41, No. 4, 102–107, 1999.
4. Furse, C. M., J.-Y. Chen, and O. P. Gandhi, "The use of the frequency-dependent finite-difference time-domain method for induced current and SAR calculations for a heterogeneous model of the human body," *IEEE Trans. Electromagn. Compat.*, Vol. 36, No. 2, 128–133, May 1994.
5. Chou, H.-H., H.-T. Hsu, H.-T. Chou, K.-H. Liu, and F.-Y. Kuo, "Reduction of peak SAR in human head for handset applications with resistive sheets (R-cards)," *Progress In Electromagnetics Research*, Vol. 94, 281–296, 2009.
6. Wang, J., O. Fujiwara, S. Kodera, and S. Watanabe, "FDTD calculation of whole-body average SAR in adult and child models for frequencies from 30 MHz to 3 GHz," *Physics in Medicine and Biology*, Vol. 51, No. 17, 4119, Aug. 2006.
7. Hirata, A., H. Sugiyama, and O. Fujiwara, "Estimation of core temperature elevation in humans and animals for whole-body averaged SAR," *Progress In Electromagnetics Research*, Vol. 99, 53–70, 2009.
8. Piuze, E., P. Bernardi, M. Cavagnaro, S. Pisa, and J. C. Lin, "Analysis of adult and child exposure to uniform plane waves at mobile communication systems frequencies (900 MHz–3 GHz)," *IEEE Trans. Electromagn. Compat.*, Vol. 53, No. 1, 38–47, Feb. 2011.
9. Capstick, M. H., N. Kuster, S. Kuehn, V. Berdinas-Torres, J. Ladbury, G. Koepke, D. McCormick, J. Gauger, and R. Melnick, "A radio frequency radiation reverberation chamber

- exposure system for rodents,” *URSI International Union of Radio Science, XXIX General Assembly 2008*, Chicago, USA, Aug. 2008.
10. Hegge, N., C. Orlenius, and P. S. Kildal, “Development of reverberation chamber for accurate measurements of mobile phones and mobile phone antennas,” *IEE Antenna Measurements and SAR, AMS 2004*, 55–58, May 2004.
 11. Wu, T., A. Hadjem, M.-F. Wong, A. Gati, O. Picon, and J. Wiart, “Whole-body new-born and young rats’ exposure assessment in a reverberating chamber operating at 2.4 GHz,” *Physics in Medicine and Biology*, Vol. 55, No. 6, 1619, 2010.
 12. Biagi, P. F., L. Castellana, T. Maggipinto, G. Maggipinto, T. Ligonzo, L. Schiavulli, D. Loiacono, A. Ermini, M. Lasalvia, G. Perna, and V. Capozzi, “A reverberation chamber to investigate the possible effects of “in vivo” exposure of rats to 1.8 GHz electromagnetic fields: A preliminary study,” *Progress In Electromagnetics Research*, Vol. 94, 133–152, 2009.
 13. Lalléchère, S., S. Girard, D. Roux, P. Bonnet, F. Paladian, and A. Vian, “Mode stirred reverberation chamber (MSRC): A large and efficient tool to lead high frequency bioelectromagnetic in vitro experimentation,” *Progress In Electromagnetics Research B*, Vol. 26, 257–290, 2010.
 14. Jung, K. B., T. H. Kim, J. L. Kimb, H. J. Doh, Y. C. Chung, J. H. Cho, and J. K. Pack, “Development and validation of reverberation-chamber type whole-body exposure system for mobile-phone frequency,” *Electromagnetic Biology and Medicine*, Vol. 27, No. 1, 73–82, Mar. 2008.
 15. Wang, J., O. Fujiwara, and T. Uda, “New approach to safety evaluation of human exposure to stochastically-varying electromagnetic fields,” *IEEE Trans. Electromagn. Compat.*, Vol. 47, No. 4, 971–976, Nov. 2005.
 16. De Leo, R., F. Moglie, V. Mariani Primiani, and A. P. Pastore, “SAR numerical analysis of the whole human body exposed to a random field,” *2009 IEEE International EMC Symposium*, 81–86, Austin, Tx, USA, Aug. 2009.
 17. [Online]. Available: <http://www.nlm.nih.gov/research/visible/visible-human.html>
 18. Hill, D. A., “Plane wave integral representation for fields in reverberation chambers,” *IEEE Trans. Electromagn. Compat.*, Vol. 40, No. 3, 209–217, Aug. 1998.
 19. Moglie, F. and A. P. Pastore, “FDTD analysis of plane waves superposition to simulate susceptibility tests in reverberation chambers,” *IEEE Trans. Electromagn. Compat.*, Vol. 48, No. 1,

- 195–202, Feb. 2006.
20. Crawford, M. L. and G. H. Koepke, “Design, evaluation, and use of a reverberation chamber for performing electromagnetic susceptibility/vulnerability measurements,” *National Bureau of Standards Technical Note 1092, Tech. Rep.*, Apr. 1986.
 21. “Electromagnetic compatibility (EMC) — Part 4: Testing and measurement techniques. Section 21: Reverberation chamber test methods,” IEC 61000-4-21.
 22. Berenger, J.-P., “A perfectly matched layer for the absorption of electromagnetic waves,” *Journal of Computational Physics*, Vol. 114, No. 2, 185–200, Oct. 1994.
 23. Musso, L., V. Berat, F. Canavero, and B. Demoulin, “A plane wave Monte Carlo simulation method for reverberation chambers,” *EMC Europe 2002, International Symposium on Electromagnetic Compatibility*, Vol. 1, 45–50, Sorrento, Italy, Sep. 2002.
 24. Papoulis, A., *Probability, Random Variables and Stochastic Processes*, McGraw Hill, New York, 1965.
 25. Mariani Primiani, V. and F. Moglie, “Numerical simulation of LOS and NLOS conditions for an antenna inside a reverberation chamber,” *Journal of Electromagnetic Waves and Applications*, Vol. 24, Nos. 17–18, 2319–2331, 2010.
 26. Gabriel, C., S. Gabriel, and E. Corthout, “The dielectric properties of biological tissues: I, II, III,” *Phys. Med. Biol.*, Vol. 41, 2231–2293, May 1996.
 27. Stogryn, A., “Equations for calculating the dielectric constant of saline water,” *IEEE Trans. Microw. Theory Tech.*, Vol. 19, No. 8, 733–736, Aug. 1971.
 28. Gradoni, G., F. Moglie, A. P. Pastore, and V. Mariani Primiani, “Numerical and experimental analysis of the field to enclosure coupling in reverberation chamber and comparison with anechoic chamber,” *IEEE Trans. Electromagn. Compat.*, Vol. 48, No. 1, 203–211, Feb. 2006.
 29. *Guide to The Expression of Uncertainty in Measurement*, International Organization for Standardization, Switzerland, 1993.
 30. Mariani Primiani, V., F. Moglie, and A. P. Pastore, “A metrology application of reverberation chambers: The current probe calibration,” *IEEE Trans. Electromagn. Compat.*, Vol. 49, No. 1, 114–122, Feb. 2007.